Check for updates

ADVANCED MATERIALS TECHNOLOGIES
www.advmattechnol.de

Scalable Synthesis of Bulk TiO_2 Hybrids Toward Efficient Li-Storage Performance in "Rocking-Chair" Type Full-Cell Assembly With High Voltage $LiNi_{0.5}Mn_{1.5}O_4$ Cathode

Shaji Jyothilakshmi, Krishnan Subramanyan, Yun-Sung Lee, and Vanchiappan Aravindan**

Exploring anode materials with outstanding safety, high capacities, and superior rate performance for lithium-ion batteries (LIBs) remains a constant objective. A simple and green synthesis method with an excellent electrochemical performance of a TiO_2 bronze/anatase hybrid is herein reported as an anode at different temperature conditions (400 °C, 450 °C, and 500 °C) for LIBs. The Li-ion insertion/extraction properties are studied in a half-cell assembly (Li/TiO_2) and subsequently in a "rocking-chair" type full-cell configuration with a high voltage $LiNi_{0.5}Mn_{1.5}O_4$ (LNMO) cathode. In both half and full-cell assemblies, all three TiO_2 hybrids exhibit promising results with an initial discharge capacity of >165 mAh g^{-1} at a current rate of 0.05 A g^{-1} along with a capacity retention of >90% after 100 cycles. The initial coulombic efficiency of ≈78% is observed for the full-cell, LNMO/TiO_2-400 °C, with a maximum energy density of 192.75 Wh kg^{-1} and good cyclability at room temperature conditions.

1. Introduction

Energy has become a topmost priority for the major international powers and the scientific community in response to the shifting global landscape. Owing to rising energy demand and the depletion of fossil fuels, there has been considerable interest in developing and improving more efficient energy storage devices.[1–3] Unquestionably, lithium-ion batteries (LIBs) have become the primary power sources for portable electronics and electric vehicles. They offer advantageous characteristics, including a long-cycle life, a high energy density, low production costs, and are malleable in design.[4,5] As an anode material for LIBs, titanates are being investigated intensively due to their superior safety in preventing Li metal plating compared to graphite, Si, Sn, or other low-voltage anodes.[6] TiO_2 has a theoretical specific capacity (335 mAh g^{-1}).[1,5,7] They have a specific capacity similar to that of graphite and because oxides have twice the density of graphite, they have double the theoretical volumetric energy density, no solid electrolyte interface (SEI) formation, and excellent high rate performance.[1,6,8–11] These potential advantages render TiO_2 attractive as an anode for LIBs. Various polymorphs of TiO_2 have been investigated as possible anodes for LIB applications, amongst which, anatase and bronze phase have secured immense attention due to their electrochemical activity in both the bulk and nanostructured forms with good cyclability compared to the rutile and brookite phases.[2,8,12] The bronze phase is a desirable contender for making high-power and high-energy density Li-ion power packs due to its reduced insertion potential (≈1.65 V vs Li), high reversibility, and high current performance compared to the anatase phase.[3,6,13–17]

Exnar et al.[18] was the first one to report a novel LIB using $LiNi_{0.5}Co_{0.5}O_2$ as a cathode and a commercially available nanocrystalline TiO_2 as an anode. The $LiNi_{0.5}Co_{0.5}O_2$/TiO_2 full-cell delivered a reversible capacity of ≈46 mAh g^{-1} (based on the total mass of the electrodes) with significant fading. Chen et al.[19] prepared TiO_2 nanotubes by a facile alkaline hydrothermal method, where commercial TiO_2 nanoparticles were employed as starting materials, then annealing at 350 °C.[2] Armstrong et al.[20] first prepared TiO_2(B) nanowires where synthesis involved initially adding the anatase TiO_2 into a 15 mol/L NaOH solution and hydrothermal treatment at 170 °C for 72 h. A modified version of this method was further reported by Kobayashi et al.[21] where metallic Titanium was dissolved in an H_2O_2 and $NH_3.H_2O$ solution under an ice/water bath; after the addition of glycolate acid and adjustment of pH value by concentrated H_2SO_4, the solution was hydrothermally heated at 160 °C for 30 min. Similarly, many works reported that titanates were generally prepared by hydrothermal reaction.[19,21,22] Yan and his group[8] successfully prepared bronze/anatase TiO_2 hybrid nanowires through the simple stirring hydrothermal process, which has elongated bending wire morphology and a heterojunction structure with TiO_2–bronze and anatase TiO_2 nanocrystals.

S. Jyothilakshmi, K. Subramanyan, V. Aravindan
Department of Chemistry
Indian Institute of Science Education and Research (IISER)
Tirupati 517507, India
E-mail: aravindan@iisertirupati.ac.in
Y.-S. Lee
School of Chemical Engineering
Chonnam National University
Gwang-ju 61186, Republic of Korea
E-mail: leeys@chonnam.ac.kr

The ORCID identification number(s) for the author(s) of this article can be found under https://doi.org/10.1002/admt.202202036

DOI: 10.1002/admt.202202036

 © 2023 Wiley-VCH GmbH

2365709x, 2023, 12, Downloaded from https://onlinelibrary.wiley.com/doi/10.1002/admt.202202036 by Chonnam National University Hwasun Hospital, Wiley Online Library on [27/12/2023]. See the Terms and Conditions (https://onlinelibrary.wiley.com/terms-and-conditions) on Wiley Online Library for rules of use; OA articles are governed by the applicable Creative Commons License

While using hydrothermal reactions, it is necessary to regulate synthesis parameters, including solution temperature, pH, reaction time, and precursor ratio.[23] Furthermore, to get highly pure and crystalline nanoparticles, lengthy reaction durations and drying procedures are required, which complicates mass production.[24] In addition, determining the atomic structure of nanosized particles is difficult because their powder diffraction peaks become severely, and sometimes anisotropically broadened, making it difficult or impossible to use established crystallographic methods.[13]

The new method reported herein is an efficient, environmentally friendly, and scalable method to produce highly pure, TiO_2 from sodium meta-titanate ($Na_2Ti_3O_7$) via simple bulk–direct synthesis employing mechanochemical processes. The novelty of this work is in the synthesis part, where we have eliminated the time-consuming, high-temperature, and expensive operation techniques, specifically no hydrothermal reaction. Hence, we strongly believe this new TiO_2 bulk synthesis method is suitable for scalable synthesis and provides a potentially impactful anode material for Li-ion storage properties. On the Li-storage properties, all the prepared TiO_2 hybrids in three different temperature conditions were employed in both half-cell and full-cell assemblies and discussed in detail.

2. Results and Discussion

Sodium meta-titanate ($Na_2Ti_3O_7$) and hydrochloric acid react through an ion exchange process with HCl to give $H_2Ti_3O_7$. The intermediate product is completely different than the conventional synthesis of the TiO_2-B phase, in which $H_2TiO_{2n+1}.xH_2O$ would be obtained after the acid washing with HCl, while the anatase phase and highly concentrated NaOH as a precursor for hydrothermal reaction. In the present case, after washing and controlled pyrolysis, $H_2Ti_3O_7$ transforms into TiO_2. The crystalline structure of synthesized TiO_2 was analyzed by powder X-ray diffraction measurements and shown in **Figure 1**a. From the XRD patterns, it is observed that all peaks are sharp, which corresponds to the high crystalline nature of the hybrid phase prepared. Further, it is evident that all the synthesized TiO_2 samples have a mixed phase, and the distinct peaks identified correspond to the anatase and bronze (B) phase; for example, the prominent peaks appearing at 25.10° and 25.27° belonged to the (110) plane of TiO_2(B) and the (101) plane of anatase TiO_2, respectively. The fractions/compositions of the bronze and anatase phases of TiO_2 in the TiO_2-400 °C, TiO_2-450 °C, and TiO_2-500 °C samples are provided in Table S1, Supporting Information. The results revealed that the amount of TiO_2(B) phase is higher in TiO_2-400 °C, whereas the anatase phase is rich in TiO_2-450 °C.

The surface elemental composition and purity of the TiO_2 hybrids have been examined using XPS. The XPS survey spectra have indicated the presence of Ti and O (Figure S1, Supporting Information). Deconvolution of the Ti 2p and O 1s has been done to determine the chemical/oxidation state of the individual elements (Figure 1b–d). The deconvolution of O 1s core level produces peaks at 531.8, 533.3, and 530.1 eV, which correspond to the C=O, C–O, and lattice oxygen functional groups, respectively.[13,25] The spectra of Ti 2p exhibit two pair of peaks belonging to the Ti $2p_{1/2}$ and Ti $2p_{3/2}$ states. This indicates that the Ti in the TiO_2 hybrids is in the 4+ oxidation state, irrespective of the calcination temperature.

To understand the surface morphological and structural features of TiO_2 hybrids, electron microscopy imaging techniques such as FE-SEM and HR-TEM have been used. The FE-SEM image (**Figure 2**a,e,i) depicts a non-uniform size distribution owing to the agglomeration of particles, with a particulate size of ≈3 µm. It was further confirmed from the TEM analysis that the particles are in bulk form (Figure 2b,f,j). The lattice fringe width or *d* spacing (Figure 2c,g,k) has been determined from the TEM image as 0.18, 0.20, and 0.18 nm for TiO_2-400 °C, TiO_2-450 °C, and TiO_2-500 °C, respectively. The selected area electron diffraction (SAED) (Figure 2g,h,l) pattern also reveals the high crystallinity of the as-synthesized TiO_2 samples. The energy dispersion X-ray spectroscopy (EDS) (Figure S2, Supporting Information) analysis depicts the uniform distribution of elements Ti and O in the sample. Therefore, the formation of TiO_2, its crystalline nature, and the bulkiness of the particles have been confirmed by all these analytical techniques such as XRD, XPS, FE-SEM, HR-TEM, and EDS studies.

2.1. Half-Cell Studies

The electrochemical performance of TiO_2 was studied through Li/TiO_2 half-cell assembly at a voltage range of 1–3 V vs. Li. Prior to the fabrication of the TiO_2 hybrids, the commercial $Na_2Ti_3O_7$ was subjected to Li-storage performance in half-cell assembly, in which negligible capacity was observed. A marginal capacity improvement was observed for the powder when it underwent high-energy ball milling. Then, we attempted to remove the Na-ions from the structure by ion-exchange reaction with HCl, which resulted in the formation of the $H_2Ti_3O_7$. Further, the hydrogen–titanate was subjected to thermal treatment to form the TiO_2–bronze phase at three different temperature conditions. The electrochemical performance of bare–NTO, ball–milled NTO, TiO_2-400 °C, TiO_2-450 °C, and TiO_2-500 °C is compared in Figure S3, Supporting Information. Cyclic voltammetry (CV) studies of the cells were carried out at different scan rates from 0.1 to 1 mV s^{-1} (**Figure 3**a,c,e). When comparing the CV of all three half-cells, two anodic peaks are found at ≈1.71 and ≈2.05 V vs. Li, which may be due to the presence of two different electrochemical contributions. Upon the cathodic scan, the peak positions were observed at ≈1.35 and ≈1.7 V vs. Li, which was associated with the Li-insertion into the bronze and anatase phases, respectively. The anodic peak positioned at ≈1.71 V vs. Li corresponds to the extraction of Li-ions from TiO_2(B), and the small peak at ≈2.05 V vs. Li belongs to the anatase phase of TiO_2.[7,22] During cathodic and anodic scans, noticeable peaks are related to the reduction (Ti^{4+}/Ti^{3+}) and oxidation (Ti^{3+}/Ti^{4+}) process of Ti, respectively.[26] It is also observed that as the scan rate increases, the peaks shift toward higher potential regions because the peak current is directly proportional to the square root of the scan rate. In addition, the second and small anodic peak observed at ≈2.05 V vs. Li tends to merge with the peak at ≈1.71 V vs. Li at a higher scan rate due to the increase in polarization at the high scan rates. Based on the observations from XRD, the CV studies also complement the presence of the anatase content, for which the anatase phase is

 © 2023 Wiley-VCH GmbH

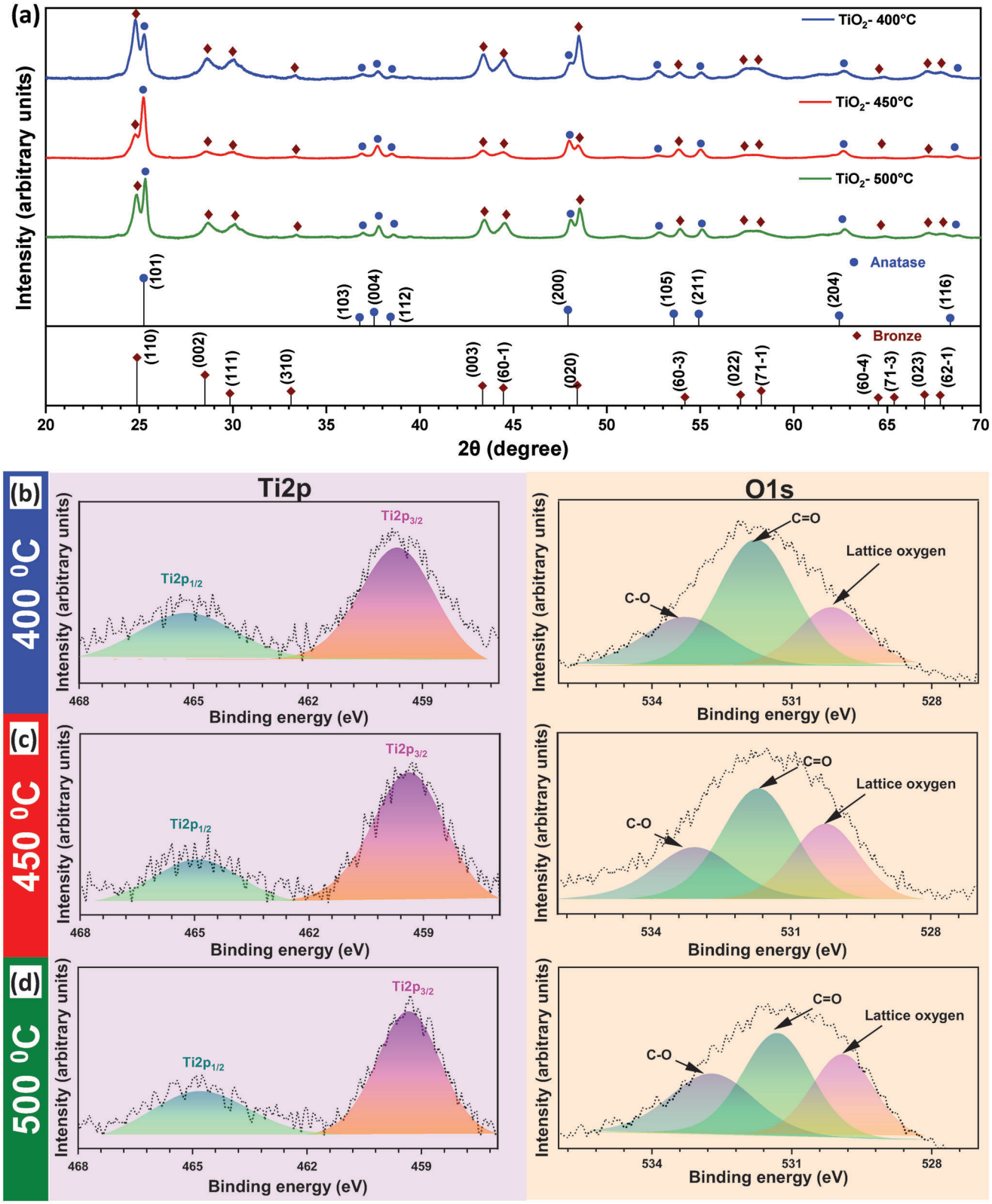

Figure 1. a) XRD pattern of TiO_2-400 °C (blue), TiO_2-450 °C (red), and TiO_2-500 °C (green), and b–d) deconvoluted XPS spectra of Ti 2p and O 1s for TiO_2-400 °C, TiO_2-450 °C, and TiO_2-500 °C.

© 2023 Wiley-VCH GmbH

2365709x, 2023, 12, Downloaded from https://onlinelibrary.wiley.com/doi/10.1002/admt.202202036 by Chonnam National University Hwasun Hospital, Wiley Online Library on [27/12/2023]. See the Terms and Conditions (https://onlinelibrary.wiley.com/terms-and-conditions) on Wiley Online Library for rules of use; OA articles are governed by the applicable Creative Commons License

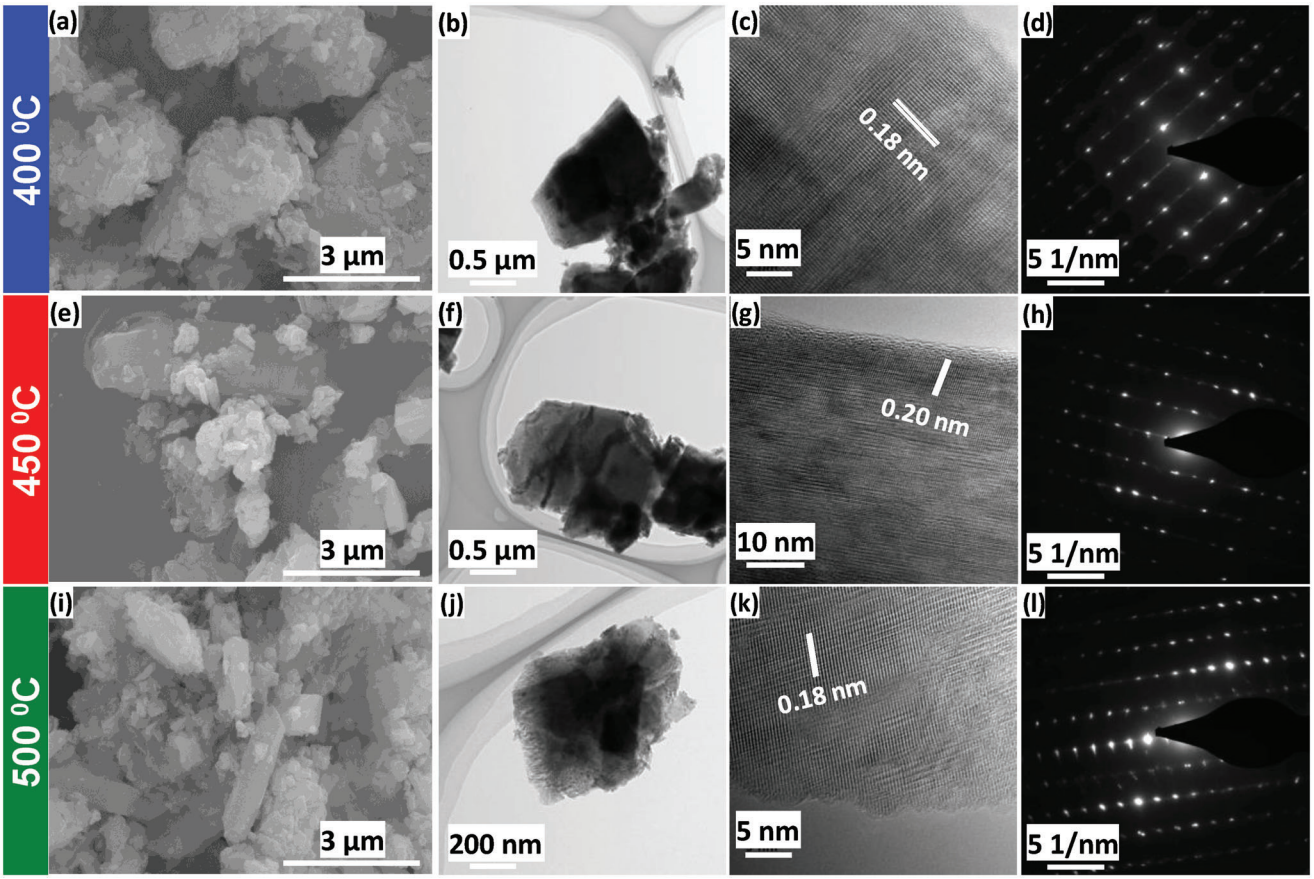

Figure 2. a,e,i) FE-SEM images of TiO_2 hybrids, b,c,f,g,j,k) HR-TEM images, and d,h,l) SAED pattern of TiO_2-400 °C, TiO_2-450 °C, and TiO_2-500 °C, respectively.

found to be highest in the TiO_2-450 °C sample, followed by TiO_2-500 °C and the least one in the TiO_2-400 °C.

The diffusion coefficient of Li^+-ions for all TiO_2 phases has also been determined from the CV by varying the scan rate from 0.1 to 1 mV s^{-1}. The diffusion coefficient is evaluated using the Randles–Sevcicks equation[12,27]

$$i_p = 2.69 \times 10^5 n^{3/2} C_0 A D^{1/2} v^{1/2} \quad (1)$$

where i_p is the peak current, n is the number of Li^+ ions involved in the electrochemical reaction, C_0 is the concentration of Li^+ ions, A is the cross-sectional area of the electrode, D is the diffusion coefficient, and v is the scan rate. A graph is plotted with the peak current observed for both cathodic as well as anodic against the square root of the scan rate (Figure 3b,d,f). Now, the apparent diffusion coefficient is calculated from the slope, $I_p/v^{1/2}$, of peak current vs. square root of the scan rate plot. From Table S2, Supporting Information, it can be observed that the magnitude of the diffusion coefficient (anodic and cathodic) for TiO_2-450 °C is ≈2.57 × 10^{-10} and ≈3.15 × 10^{-10} cm^2 s^{-1}, which is much higher compared to the diffusion coefficient of TiO_2-500 °C (≈1.65 ×10^{-10} and ≈1.70 × 10^{-10} cm^2 s^{-1}) and TiO_2-400 °C (≈1.46 ×10^{-10} cm^2 s^{-1} for both cases).

The galvanostatic rate performance of all three samples was evaluated in half-cell configuration with current densities varying from 0.05 to 1.5 A g^{-1} (**Figure 4**). Typical galvanostatic charge–discharge (GCD) curves for rate performance (Figure 4a,c,e) exhibit a similar manner for all three samples. A small biphase/flat plateau is visible at ≈2.05 V vs. Li, which is associated with the Li^+ ions extraction from the anatase phase and in good agreement with the results observed from CV curves, for example, TiO_2-450 °C and TiO_2-500 °C. As the current density increases, the biphase plateau is eventually disappearing, for example, TiO_2-400 °C. This resonates with the merging of the CV peaks at a high scan rate for TiO_2-400 °C. A smooth/monotonous slope in the voltage range of ≈1.6 V vs. Li was observed, which mainly corresponds to the insertion of Li-ion into the TiO_2(B) phase.[13] The rate performance of all three TiO_2 in half cells exhibited promising results with increasing current rates (Figure 4b,d,f). At a higher current of 1.5 A g^{-1}, Li/TiO_2-400 °C, Li/TiO_2-450 °C, and Li/TiO_2-500 °C half–cells displayed a discharge capacity of 26, 50, and 38 mAh g^{-1}, respectively. When all half cells were switched to 0.05 A g^{-1} after cycling at a higher current of 1.5 A g^{-1}, the retention of 90, 94, and 92% of initial capacity was observed, respectively, which suggests excellent structural stability and capacity retention characteristics. We strongly believe the exceptional performances at high current rates are mainly attributed to its crystal structure due to the presence of the TiO_2 bronze phase. In the rate performance study, TiO_2-450 °C dominates the other samples in terms of capacity at high current and capacity retention after

© 2023 Wiley-VCH GmbH

2365709x, 2023, 12, Downloaded from https://onlinelibrary.wiley.com/doi/10.1002/admt.202202036 by Chonnam National University Hwasun Hospital, Wiley Online Library on [27/12/2023]. See the Terms and Conditions (https://onlinelibrary.wiley.com/terms-and-conditions) on Wiley Online Library for rules of use; OA articles are governed by the applicable Creative Commons License

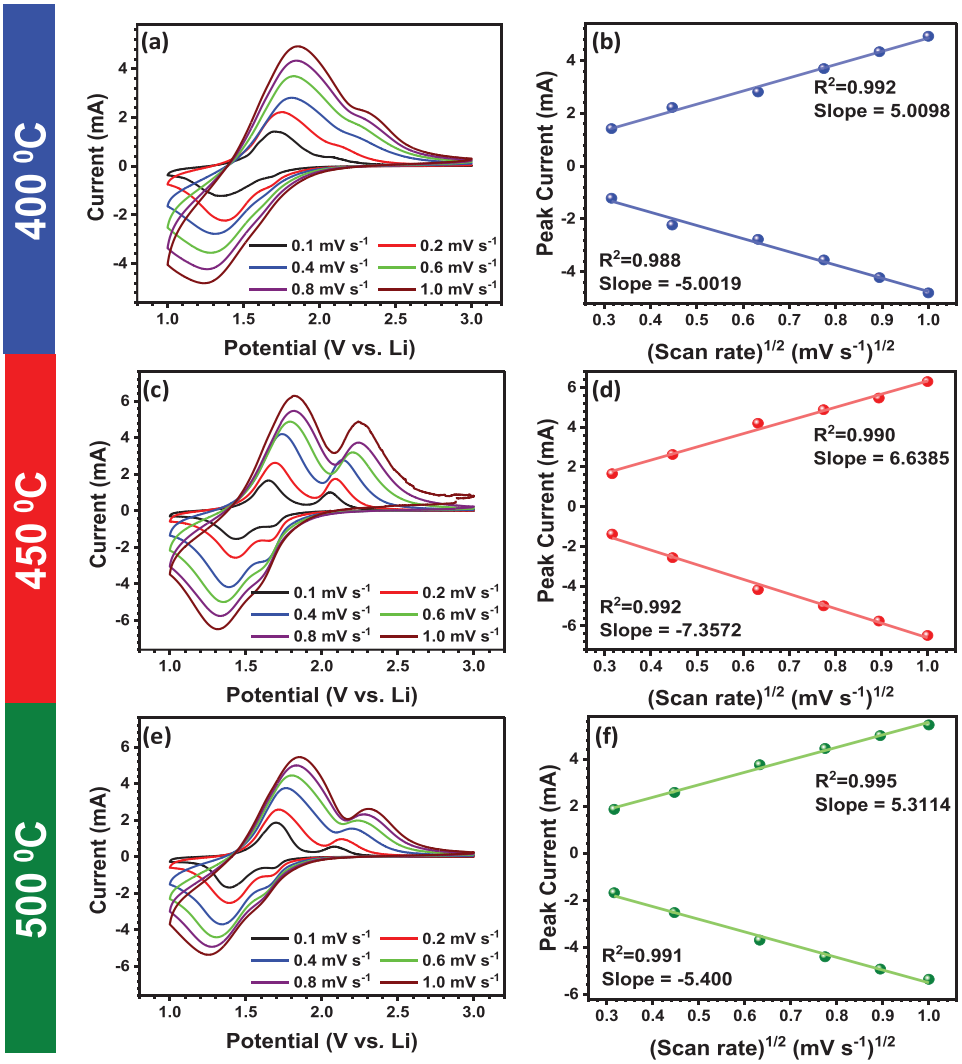

Figure 3. a,c,e) Cyclic voltammetry curves of TiO_2 half–cells, and b,d,f) Plot of peak current vs square root of scan rate.

the high current testing. A cycling profile at 0.05 A g^{-1} for 100 cycles was performed for all the half-cells. The cells render a discharge capacity of 149, 168, and 154 mAh g^{-1} (with a capacity retention of 80%, 94%, and 84%) after 100 cycles for TiO_2-400 °C, TiO_2-450 °C, and TiO_2-500 °C, respectively. The initial coulombic efficiency (ICE) of the three cells was found to be 86%, 93%, and 91% as well. In terms of specific capacity, capacity retention, and ICE, the TiO_2-450 °C hybrid was superior compared to TiO_2 synthesized at other temperature conditions. The GCD curves of the half-cells for the cycling test are shown in Figure S4, Supporting Information. SEM images of the TiO_2 electrodes and the TiO_2: acetylene black: TAB-2 powder scratched (and intact with current collector) off from the electrode post-cycling are shown in Figure S5, Supporting Information. No noticeable change in the morphology of the TiO_2 particles could be observed. Pre and post-cycling Nyquist plots for all the TiO_2-400 °C, TiO_2-450 °C, and TiO_2-500 °C samples are given in Figures S6 and S7, Supporting Information, respectively. The charge transfer resistance (R_{ct}) values before cycling are found to be 106.1, 75.41, and 94.32 ohms for TiO_2-400 °C, TiO_2-450 °C, and TiO_2-500 °C, respectively. The XRD pattern of TiO_2-450 °C after lithiation have been recorded and compared with the pristine TiO_2-450 °C (Figure S8, Supporting Information). Prominent peak shifts toward lower 2θ values and merging of peaks were observed, confirming the lithiation into the TiO_2 phases.

From the half–cell studies, it is evident that TiO_2-450 °C shows better electrochemical performance, including rate capability, stability, and capacity retention, which is primarily due to its distinctive structure. The ratio of TiO_2 bronze and anatase phases helps TiO_2-450 °C to display extraordinary performance.[12] It is well known that the bronze phase's electrical conductivity is inferior compared to the anatase phase. The 450 °C sample is composed of a larger anatase phase, resulting in better electrical conductivity. As a result, the hybrids synthesized at 450 °C render better electrochemical activity, especially at higher rates.[6]

The exceptional performance of TiO_2 hybrids logically led us to demonstrate the possibility of fabricating the "rocking-chair" type full-cell with commercial cathodes. Accordingly, we have

© 2023 Wiley-VCH GmbH

2365709x, 2023, 12, Downloaded from https://onlinelibrary.wiley.com/doi/10.1002/admt.202202036 by Chonnam National University Hwasun Hospital, Wiley Online Library on [27/12/2023]. See the Terms and Conditions (https://onlinelibrary.wiley.com/terms-and-conditions) on Wiley Online Library for rules of use; OA articles are governed by the applicable Creative Commons License

2365709x, 2023, 12, Downloaded from https://onlinelibrary.wiley.com/doi/10.1002/admt.202202036 by Chonnam National University Hwasun Hospital, Wiley Online Library on [27/12/2023]. See the Terms and Conditions (https://onlinelibrary.wiley.com/terms-and-conditions) on Wiley Online Library for rules of use; OA articles are governed by the applicable Creative Commons License

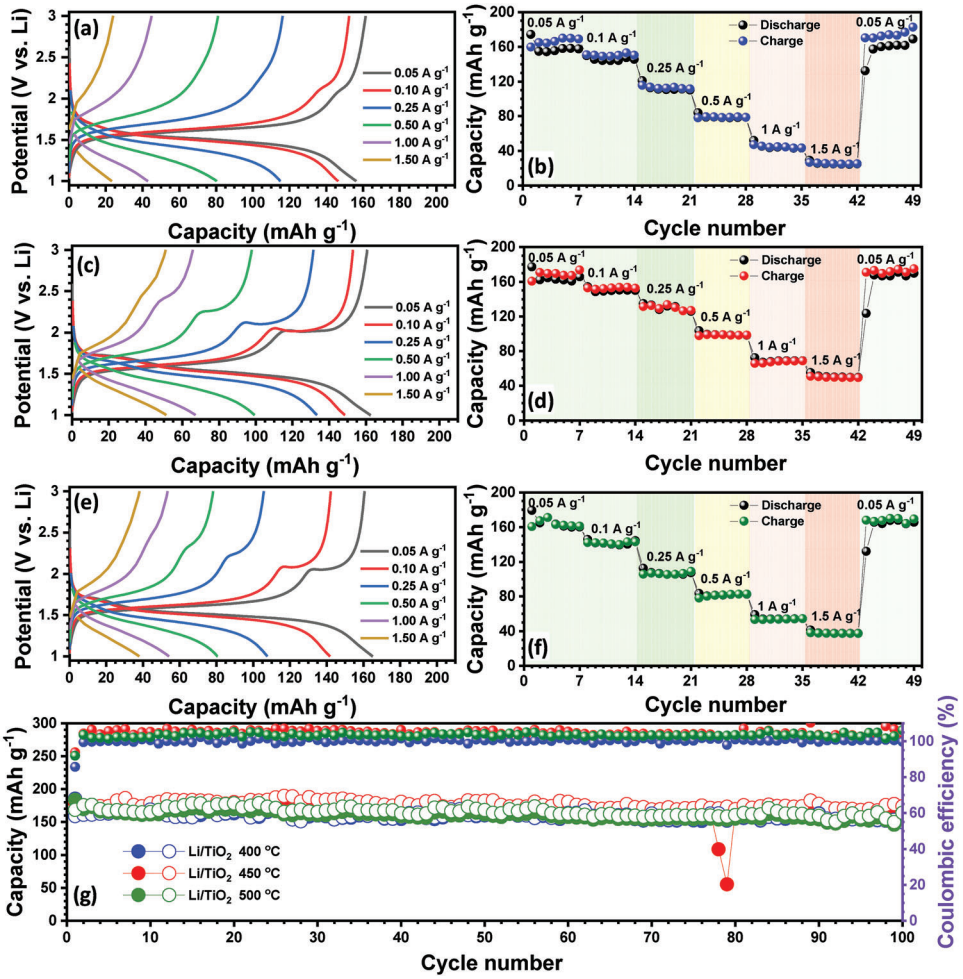

Figure 4. Half–cell performance of TiO_2 hybrids: galvanostatic charge–discharge curves and rate performance for a,b) TiO_2-400 °C, c,d) TiO_2-450 °C, e,f) TiO_2-500 °C, and g) long-term cycling of all TiO_2 half–cells between 1 and 3 V vs Li at a current density of 0.05 A g^{-1} along with Coulombic efficiency. Open and filled symbols correspond to charge and discharge, respectively, whereas the spheres belong to efficiency.

chosen high voltage spinel $LiNi_{0.5}Mn_{1.5}O_4$ (LNMO) as a cathode/counter electrode for TiO_2. Before assembling the full-cells, the Li–insertion/extraction of the commercially available LNMO cathode was investigated in half-cell configuration between 3.5 and 5 V vs. Li. These half-cell studies are essential to balance the loading between the anode and cathodes. CV traces at different scan rates (0.1, 0.2, 0.4, 0.6, 0.8, and 1 mV s^{-1}) were recorded and illustrated in Figure S9a, Supporting Information. Apparently, the two anodic peaks (one prominent and one weak) were observed at ≈4.8 and 4 V vs. Li, which corresponds to the oxidation of Ni^{2+} to Ni^{4+} and Mn^{3+} to Mn^{4+}, respectively.[26,28] The presence of a redox couple at ≈4 V vs. Li is indicative that the LNMO belongs to the disordered structure. The spinel cathode exhibited promising rate performance by reverting to initial capacity at a current density of 0.05 A g^{-1} with a capacity retention of 91% after cycling at a higher rate of 1 A g^{-1} (Figure S9b,c, Supporting Information). The GCD curves of LNMO parallel the information obtained from CV curves. As mentioned, a small irregularity was observed at ≈4 V vs. Li due to the presence of Mn^{3+}. Long-term cyclability was tested at a current density of 0.05 A g^{-1}, and the half–cell delivered an initial capacity of 124 mAh g^{-1} with an initial coulombic efficiency of 60%, which drastically improved to 94% from the subsequent cycles. The cell retained 95% of its initial capacity even after 100 cycles (Figure S9d,e, Supporting Information).

2.2. Full-Cell Studies

We further evaluated the performance of the as-synthesized samples of TiO_2 hybrids as anode and LNMO as the cathode in full-cell assembly. "Rocking-chair" type full-cell was fabricated with optimized mass loading of the cathode active material with respect to anode active material mass and capacity, which has been estimated through the half-cell performance of individual electrodes (Figure S10, Supporting Information). The electrochemical performance of full-cell assemblies was tested at a voltage range of 2.1 to 3.6 V. The following equation explains the mechanism involved in the cells,

$$TiO_2 + Li^+ + e^- \rightarrow LiTiO_2 \approx 1.55V\,vs.Li \quad (2)$$

$$LiNi_{0.5}Mn_{1.5}O_4 \rightarrow Ni_{0.5}Mn_{1.5}O_4 + Li^+ + e^- \approx 4.70Vvs.Li \quad (3)$$

 © 2023 Wiley-VCH GmbH

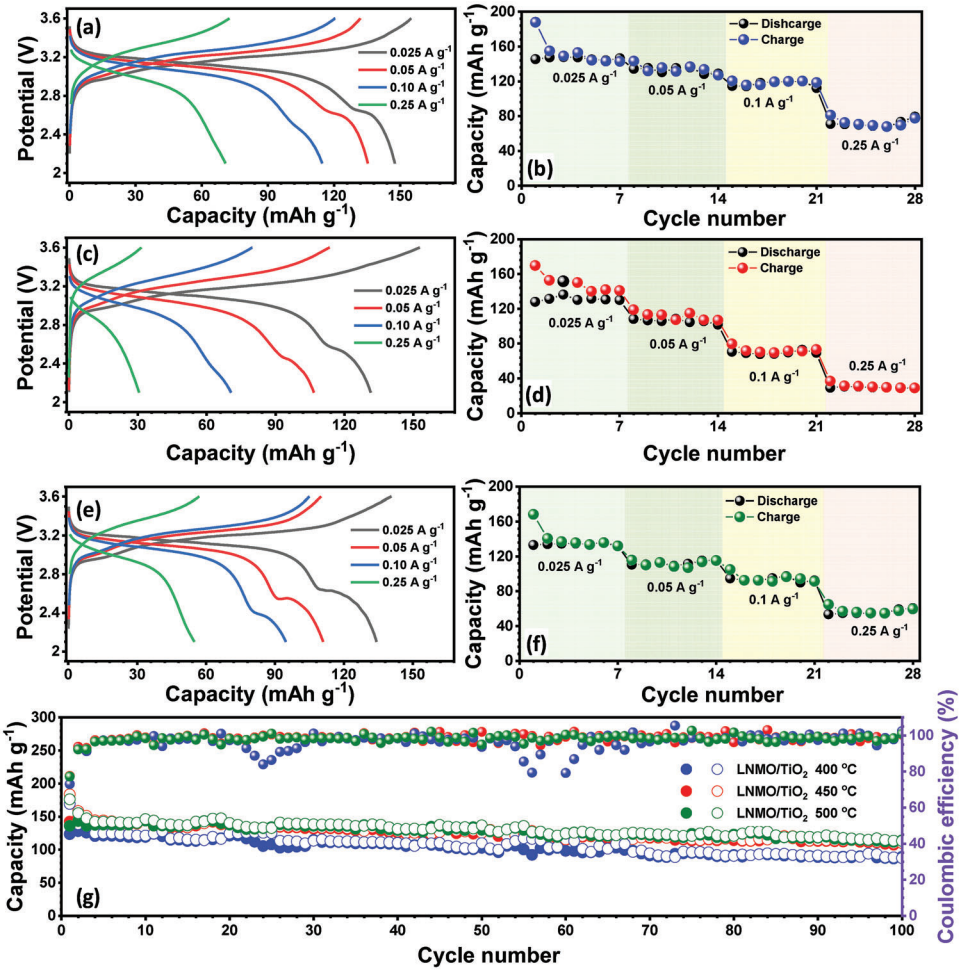

Figure 5. Full-cell performance of all LNMO/TiO_2 cells: charge–discharge curves for rate performance and rate performance of a,b) LNMO/TiO_2-400 °C, c,d) LNMO/TiO_2-450 °C, and e,f) LNMO/TiO_2-500 °C), and g) long-term cycling profile of all full–cells between 2.1 and 3.6 V at a current density of 0.05 A g^{-1} along with Coulombic efficiency. Open and filled symbols correspond to charge and discharge, respectively, whereas the spheres belong to efficiency.

$$LiNi_{0.5}Mn_{1.5}O_4 + TiO_2 \rightarrow Ni_{0.5}Mn_{1.5}O_4 + LiTiO_2 \approx 3.15\ V \quad (4)$$

The specific capacity and applied current densities are calculated based on the anode active material mass loading. During rate performance (**Figure 5**b,d,f), despite the TiO_2 half-cells showing noteworthy capacity at high currents, the full-cells were unable to maintain a high capacity at current rates beyond 0.25 A g^{-1}. It is clearly evident in half-cell studies of LNMO that rate performance is very poor at higher current rates. The full-cell was cycled at 0.05 A g^{-1} (Figure 5g), where the LNMO/TiO_2-400 °C, LNMO/TiO_2-450 °C, and LNMO/TiO_2-500 °C-based cells displayed a discharge capacity of ≈88, ≈109, and ≈113 mAh g^{-1} after 100 cycles (with corresponding capacity retention of 70, 76, and 83%), respectively. The ICE is fairly good for the full-cell assemblies, indicating the absence of any major irreversible processes. Coulombic efficiencies increase beyond 92% for all three cells from the second cycle onwards. The GCD curves of the full–cells for the long-term cycling test are shown in Figure S11, Supporting Information.

A Ragone plot for the full-cells was also constructed with specific energy and power densities at different current rates. The energy and power densities were calculated based on the anode's and cathode's total active material mass (**Figure 6**). The details of the energy and power density calculation are given in the Supporting Information. The LNMO/TiO_2-400 °C cell exhibited a maximum energy density of 192.75 Wh kg^{-1} (@ power density of 16.07 W kg^{-1}). LNMO/TiO_2-450 °C and LNMO/TiO_2-500 °C cells showed slightly lower energy densities of 169.18 and 175.62 Wh kg^{-1}, respectively. This uneven variation in energy density and power density may be due to the uneven composition of anatase and bronze phases in TiO_2 for all three samples. In terms of capacity, ICE, and energy density, LNMO/TiO_2-400 °C full-cell showed better performance. Other assemblies also displayed reasonable performance at lower current rates, which is clearly seen from the Ragone plot. However, especially at higher rates, the LNMO/TiO_2-400 °C assembly failed to translate the comparable performance. Further studies are in progress to minimize the anatase phase in the hybrid to yield the pure phase compound, that is, the bronze phase, by fine-tuning the synthesis protocols.

© 2023 Wiley-VCH GmbH

2365709x, 2023, 12, Downloaded from https://onlinelibrary.wiley.com/doi/10.1002/admt.202202036 by Chonnam National University Hwasun Hospital, Wiley Online Library on [27/12/2023]. See the Terms and Conditions (https://onlinelibrary.wiley.com/terms-and-conditions) on Wiley Online Library for rules of use; OA articles are governed by the applicable Creative Commons License

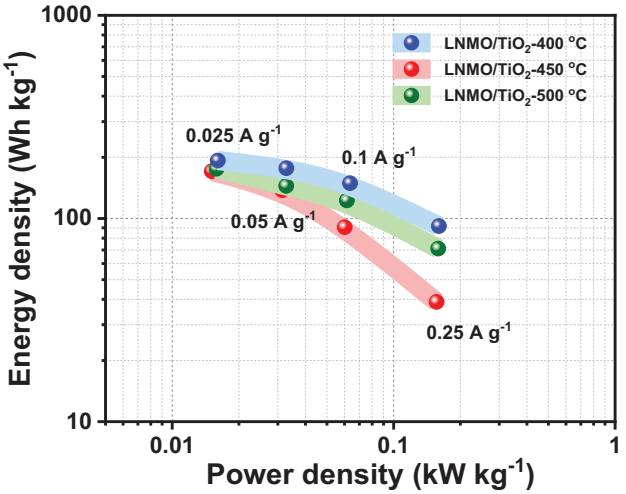

Figure 6. Ragone plot for all three LNMO/TiO_2 full-cells based on the total active material mass of anode and cathode.

In terms of application perspective, the focus is to improve the reversible Li-insertion/extraction process, which eventually leads to an increase in the net energy density of the cell.

3. Conclusion

In this work, we have successfully synthesized bulk TiO_2 hybrids from sodium meta-titanate (NTO) through a facile mechano-chemical and ion-exchange process under different temperature conditions. We have observed that the as-synthesized sample consists of both bronze and anatase phases of TiO_2 and studied the Li-storage properties of such hybrids in both half and full-cell (with spinel LNMO cathode) assemblies in a comparative way. Prior to the fabrication of the full-cell, the mass loading between the anode to cathode was adjusted based on the half-cell performance. The full-cell assembled with LNMO/TiO_2-400 °C exhibited the maximum energy density of 194.75 Wh kg^{-1} with good cyclability. This synthesis method opens up new avenues for the synthesis of bulk bronze phase TiO_2 anodes in a scalable and eco-friendly manner by escalating the conventional synthesis using the high-intense hydrothermal reaction. The anatase phase is inevitably present in all the phases, but it is beneficial to attain better electrochemical activity of the TiO_2 hybrids; though, it offers an elevated insertion potential.

4. Experimental Section

To prepare TiO_2, commercially available sodium meta-titanate ($Na_2Ti_3O_7$ – NTO) was subjected to high–energy mechanical milling (HEMM) for 30 min. 500 mg of this ball-milled NTO was added to 30 mL HCl and stirred overnight at 450 rpm at room temperature. The resulting content was centrifuged and washed with deionized water until the pH became neutral. The intermediate product was thermally treated in a box furnace (Carbolite, UK) in an air atmosphere for 5 h at different temperature conditions (400 °C, 450 °C, and 500 °C). LNMO had been purchased commercially (MTI, USA) and used directly without any further purification.

Material Characterizations: Power X-ray diffraction (XRD) measurements were conducted to identify the crystalline nature and composition of TiO_2. Rigaku Smartlab automated multipurpose X-ray diffractometer with a monochromatic Cu Kα radiation (λ = 1.5604 Å) was used to study the crystallographic parameters of TiO_2 with a scan rate of 2° min^{-1}. The surface composition and oxidation states of TiO_2 hybrids were analyzed through high–resolution X-ray photoelectron spectroscopy (XPS, multilab instrument with a monochromatic Al Kα radiation hυ = 1486.6 eV, 2000, UK). The particle morphology characterizations, size, and composition of TiO_2 were studied using a field emission scanning electron microscope (FE–SEM, S–4700, Hitachi, Japan) and a high-resolution transmission electron microscope (HR-TEM, TECNAI, Philips, the Netherlands, 200 keV). Elemental composition analysis was performed with the help of energy dispersive X-ray spectroscopy (EDS).

Electrochemical Characterization: *Electrode Fabrication of TiO_2 and $LiNi_{0.5}Mn_{1.5}O_4$ (LNMO)*: Both electrodes were prepared manually using a mortar and pestle. 10 mg active material (TiO_2), 2 mg acetylene black, and 2 mg teflonized acetylene black (TAB–2, binder) were mixed together in ethanol until a free-standing film was formed. This was pressed onto a stainless steel (Nominal aperture: 0.38 mm, Goodfellow, UK) mesh of 14 mm diameter using a hydraulic press (Specac, UK) and kept in a vacuum oven at 75 °C for at least 4 h before cell fabrication. The average electrode thickness was ≈16.5 µm, with a mass loading of ≈6.5 mg cm^{-2}. The stainless–steel mesh acts as a current collector for the electrode. Similarly, the LNMO electrodes for full–cell experiments were prepared, with the active material loading adjusted to balance the anode's capacity, in which the ratio of TiO_2:LNMO was fixed to be 1:≈1.4.

Half and Full-Cell Fabrication: Half cells of TiO_2 and LNMO were fabricated using lithium metal as reference and counter electrodes for electrochemical testing. Both half and full-cells use 1 M lithium hexafluorophosphate in ethylene carbonate–dimethyl carbonate (EC:DMC) in 1:1 vol.% as electrolyte ($LiPF_6$, LIPASTE, Tomiyama). The anode areal mass loading of active material for the half–cell was ≈6.5 mg cm^{-2}. A glass microfiber filter paper (Whatmann, cat no. 1825–047, UK) had been used as a separator. Full–cell assembly was made using all three TiO_2 as anode and LNMO as a cathode. TiO_2 phase was mixed as anode and LNMO as a cathode under balanced loading conditions. Both half and full–cells had been fabricated in an inert atmosphere (Glove box, MBraun, Germany, O_2 < 0.1 ppm and H_2O < 0.1 ppm). Electrochemical testing for half-cells and full–cells was carried out using the BioLogic battery tester (BCS–805) at ambient temperature conditions.

Supporting Information

Supporting Information is available from the Wiley Online Library or from the author.

Acknowledgements

S.J. and K.S. contributed equally to this work. S.J. thanks the University Grants Commission for the Junior Research Fellowship (KL05600139) and the Prime Minister's Research Fellowship (0902009). K.S. thanks the Department of Science & Technology (DST), Govt. of India, for the financial support through INSPIRE fellowship (IF180157). Y.S.L. acknowledges the financial support from the National Research Foundation of Korea (NRF) grant funded by the Korean government (Ministry of Science, ICT&Future Planning) (No. 2019R1-A2C1007620). V.A. acknowledges financial support from the Science and Engineering Research Board, a statutory body of DST, Govt. of India, through Swarnajayanti Fellowship (SB/SJF/2020-21/12)

Conflict of Interest

The authors declare no conflict of interest.

Data Availability Statement

The data that support the findings of this study are available from the corresponding author upon reasonable request.

© 2023 Wiley-VCH GmbH

2365709x, 2023, 12, Downloaded from https://onlinelibrary.wiley.com/doi/10.1002/admt.202202036 by Chonnam National University Hwasun Hospital, Wiley Online Library on [27/12/2023]. See the Terms and Conditions (https://onlinelibrary.wiley.com/terms-and-conditions) on Wiley Online Library for rules of use; OA articles are governed by the applicable Creative Commons License

Keywords

anodes, bronze & anatase, high-voltage, hybrids, insertion, Li-ion batteries

Received: December 7, 2022
Revised: January 28, 2023
Published online: April 4, 2023

[1] O. Game, T. Kumari, U. Singh, V. Aravindan, S. Madhavi, S. B. Ogale, *Energy Storage Mater.* **2016**, *3*, 106.
[2] B. Zachau-Christiansen, K. West, T. Jacobsen, S. Atlung, *Solid State Ionics* **1988**, *28–30*, 1176.
[3] D. P. Opra, S. V Gnedenkov, S. L. Sinebryukhov, *J. Power Sources* **2019**, *442*, 227225.
[4] M. Madian, A. Eychmüller, L. Giebeler, *Batteries* **2018**, *4*, 7.
[5] V. Aravindan, Y. S. Lee, R. Yazami, S. Madhavi, *Mater. Today* **2015**, *18*, 345.
[6] S. Liang, X. Wang, R. Qi, Y.-J. Cheng, Y. Xia, P. Müller-Buschbaum, X. Hu, *Adv. Funct. Mater.* **2022**, *32*, 2201675.
[7] M. Søndergaard, K. J. Dalgaard, E. D. Bøjesen, K. Wonsyld, S. Dahl, B. B. Iversen, *J. Mater. Chem. A* **2015**, *3*, 18667.
[8] X. Yan, W. Liu, W. Yan, D. Sun, Y. Jin, J. Wang, L. Xiang, H. Munakata, K. Kanamura, *Electrochim. Acta* **2016**, *191*, 661.
[9] J. Liu, W. Liu, S. Ji, Y. Wan, H. Yin, Y. Zhou, *Eur. J. Inorg. Chem.* **2014**, *2014*, 2073.
[10] J. Liu, W. Liu, K. Chen, S. Ji, Y. Zhou, Y. Wan, D. Xue, P. Hodgson, Y. Li, *Chem. - Eur. J.* **2013**, *19*, 9811.
[11] L. Yu, J. Liu, X. Xu, L. Zhang, R. Hu, J. Liu, L. Ouyang, L. Yang, M. Zhu, *ACS Nano* **2017**, *11*, 5120.
[12] M. Wagemaker, R. van de Krol, A. P. M. Kentgens, A. A. van Well, F. M. Mulder, *J. Am. Chem. Soc.* **2001**, *123*, 11454.
[13] Z. Liu, Y. G. Andreev, A. R. Armstrong, S. Brutti, Y. Ren, P. G. Bruce, *Prog. Nat. Sci.: Mater. Int.* **2013**, *23*, 235.
[14] V. Aravindan, N. Shubha, W. C. Ling, S. Madhavi, *J. Mater. Chem. A* **2013**, *1*, 6145.
[15] J. Ming, Y. Wu, S. Nagarajan, D.-J. Lee, Y.-K. Sun, F. Zhao, *J. Mater. Chem.* **2012**, *22*, 22135.
[16] H. Ming, P. Kumar, W. Yang, Y. Fu, J. Ming, W.-J. Kwak, L.-J. Li, Y. Sun, J. Zheng, *ACS Sustainable Chem. Eng.* **2015**, *3*, 3086.
[17] H. Xue, Y. Wu, Y. Zou, Y. Shen, G. Liu, Q. Li, D. Yin, L. Wang, J. Ming, *Adv. Funct. Mater.* **2020**, *30*, 1910657.
[18] I. Exnar, L. Kavan, S. Y. Huang, M. Grätzel, *J. Power Sources* **1997**, *68*, 720.
[19] H. Chen, D. Chen, L. Bai, K. Shu, *Int. J. Electrochem. Sci.* **2018**, *13*, 2118.
[20] A. R. Armstrong, G. Armstrong, J. Canales, P. G. Bruce, *Angew. Chem., Int. Ed.* **2004**, *43*, 2286.
[21] M. Kobayashi, V. V Petrykin, M. Kakihana, K. Tomita, M. Yoshimura, *Chem. Mater.* **2007**, *19*, 5373.
[22] A. Wang, Y. Wang, W. Yu, Z. Huang, Y. Fang, L. Long, Y. Song, M. P. Cifuentes, M. G. Humphrey, L. Zhang, J. Shao, C. Zhang, *RSC Adv.* **2016**, *6*, 20120.
[23] S. Mehraz, W. Luo, J. Swiatowska, B. Bezzazi, A. Taleb, *Materials* **2021**, *14*, 916.
[24] S. Yadav, A. Sharma, *J. Energy Storage* **2021**, *44*, 103295.
[25] N. Díez, A. Śliwak, S. Gryglewicz, B. Grzyb, G. Gryglewicz, *RSC Adv.* **2015**, *5*, 81831.
[26] M. Fehse, F. Fischer, C. Tessier, L. Stievano, L. Monconduit, *J. Power Sources* **2013**, *231*, 23.
[27] S. Brutti, J. Manzi, D. Meggiolaro, F. M. Vitucci, F. Trequattrini, A. Paolone, O. Palumbo, *J. Mater. Chem. A* **2017**, *5*, 14020.
[28] N. Arun, V. Aravindan, S. Jayaraman, N. Shubha, W. C. Ling, S. Ramakrishna, S. Madhavi, *Nanoscale* **2014**, *6*, 8926.

© 2023 Wiley-VCH GmbH

2365709x, 2023, 12, Downloaded from https://onlinelibrary.wiley.com/doi/10.1002/admt.202202036 by Chonnam National University Hwasun Hospital, Wiley Online Library on [27/12/2023]. See the Terms and Conditions (https://onlinelibrary.wiley.com/terms-and-conditions) on Wiley Online Library for rules of use; OA articles are governed by the applicable Creative Commons License